Ann. Occup. Hyg., Vol. 52, No. 1, pp. 23–34, 2008

doi:10.1093/annhyg/mem059

Combined Single-Drop and Rotating Drum Dustiness Test of Fine to Nanosize Powders Using a Small Drum

THOMAS SCHNEIDER* and KELD ALSTRUP JENSEN

National Research Institute for the Working Environment, Copenhagen DK-2100, Denmark

Received 5 July 2007; in final form 11 October 2007; published online 1 December 2007

A dustiness test has been developed that performs both a single-drop and a continuous rotation test using a 6-g sample. Tests were completed on pigment-grade and ultrafine TiO_2, two grades of corundum (Aloxite), yttrium-stabilized zirconia (Y-zirconia) granules, fumed silica, goethite, talc and bentonite. The generated particles were quantified by counting and sizing at 1-s time resolution using the TSI Fast Mobility Particle Sizer and the TSI Aerodynamic Particle Sizer and by collecting the particles on a filter for weighing. The method generated reproducible amounts and size distributions of particles. The size distributions had two more or less separated size modes >0.9 μm and in addition all materials except TiO_2 pigment-grade and Aloxite F1200 generated a size mode in the range from ~100 to ~220 nm. Pigment-grade TiO_2 had the lowest dustiness and ultrafine TiO_2 the highest dustiness as measured by particle number for both the single-drop and rotation test and as measured by mass for both tests combined. The difference was a factor of ~300. Three types of dust generation rate time profiles were observed; brief initial burst (talc, both grades of corundum), decaying rate during rotation period (fumed silica, TiO_2 ultrafine and pigment grade, bentonite) and constant rate (Y-zirconia, goethite). These profile types were in agreement with the differences in the ratio of amount of particles generated during the single drop to the amount generated during the single-drop and rotation test combined. The ratio ranged a factor ~40. The new test method enables a characterization of dustiness with relevance to different user scenarios.

Keywords: dustiness measurement; nanoparticles; size distributions

INTRODUCTION

Handling powdered, granular or pelletized materials generates dust. The amount and size distribution of generated particles will depend on the material-handling scenario and on the properties of the material. Many different laboratory test methods for quantifying dustiness, i.e. dustiness tests, have been developed using many different approaches for simulating real handling scenarios (Gill *et al.*, 2006). Ranking of dustiness as measured by a given method has been found to be associated with ranking of dust exposures during handling of the material (Breum *et al.*, 2003; Brouwer *et al.*, 2006; Madsen *et al.*, 2006). Dustiness is also a key parameter for assessing the risk of dust explosions (e.g. Cashdollar, 2000; Eckhoff, 2005).

The results obtained by the different dustiness test methods may not be directly comparable. A major step forward in dustiness testing was the recent publication of a European standard EN 15051 (CEN, 2006) on dustiness testing in relation to workplace exposure (Liden, 2006). This standard defines a dustiness index as the mass ratio of generated dust in milligrams to the mass of test sample in kilograms. The dustiness index may be obtained by two methods: one based on the rotating drum and another based on the continuous single-drop principle. Users of this standard should choose the one of the two methods that is most appropriate for the material and handling process they wish to simulate.

Rotating drum dustiness tests are usually performed as three replicate tests and need quite large amounts of test material, typically 300–600 g. Key characteristics of some benchtop rotating drum testers are given in Table 1. The EN 15051 continuous single-drop method requires a total amount of 500 g for the required five single-test runs. Such large amounts of test material may not be practical if very

*Author to whom correspondence should be addressed.
Tel: +45 39165295; fax: +45 39165202;
e-mail: tsc@nrcwe.dk

The free full text of this article can be found in the online version of this issue.

toxic and/or costly materials are to be tested. Therefore, there is a need for test systems that can be operated under controlled atmospheric environments using much smaller amounts of material. Previously, a fluidization method has been developed for testing nanosize powders (Maynard, 2002; Baron *et al.*, 2003; Maynard *et al.*, 2004). Fluidization was obtained by placing milligram amounts of material with or without 70-μm bronze beads in a centrifuge tube agitated by a vortex shaker. By this technique, the dustiness as a function of the force applied to the powder can be studied. Boundy *et al.* (2006) developed an air jet dispersion method for dustiness testing of pharmaceutical powders, also using only milligram amounts of sample material. The principle was to disperse the powder by a nozzle and injecting it into a glass jar for subsequent quantification.

The EN 15051 defines a classification according to the dustiness index as obtained with the rotating drum and the continuous drop method, respectively, and for both the respirable, thoracic (rotating drum only) and inhalable size fractions of the generated dust, respectively. Table 2 shows the dustiness index classes, the classification of the example materials and their actual dustiness indices as given in EN 15051. It is apparent that classification is different for the different size fractions and that the two testing principles led to different classification and different ranking within each class. These two methods have been further explored by Mareels and Pensis (2006). Using 43 samples of industrial minerals, they found that for 60% of the samples the inhalable dustiness was ranked differently by the two methods. For the respirable dustiness, it was 50%. Hamelmann and Schmidt (2004) tested the dustiness of limestone, aluminium oxide and fumed silica using both the Heubach Dustmeter (DIN, 2006) and the single-drop apparatus PALAS® Dust View. They found that also these two methods ranked the dustiness differently. More work is clearly needed for assessing the effect of different dust-producing methods on dustiness and particle size distribution, both in general and specifically regarding differences between the single drop, continuous single-drop and the rotating drum method. To facilitate such studies, Burdett *et al.* (2000) developed a test apparatus where a single-drop facility was added on a rotating drum. The apparatus consisted of a 60-cm drop tower placed on top of the drum used

Table 1. Key characteristics of some benchtop rotating drum testers

	Diameter (cm)	Length, cylindric part (cm)	Lifter vanes	Amount per single-test run	Rpm	Duration (min)	Volumetric flow rate (lpm)
MDHS 81 (HSE, 1996)	30	23	8	200 g	30	1	38
Heubach Dustmeter[a]	13.9	18.0	3	100 g	30 or 45	5	20
EN 15051 (CEN, 2006)	30	23	8	35 cm^3	4	1	38
Present method	16.3	23	3	6 g	11	1[b]	11

[a]DIN 55992-1 (2006). Parameter values in the standard can be changed if agreed upon.
[b]Preceded by a single drop.

Table 2. Classification of respirable and inhalable dustiness obtained with the rotating drum and the continuous drop method as given in EN 15051 (2006)

Dustiness	Rotating drum						Continuous drop			
Index	Material	Respirable dustiness	Material	Thoracic dustiness	Material	Inhalable dustiness	Material	Respirable	Material	Inhalable dustiness
Very low	Sulphur	3	Sulphur	5	Aloxite F1200	170	Sulphur	<LOD[a]	Aloxite F1200	200
Low	Aloxite F1200	40	Aloxite F1200	140	Sulphur	220	Aloxite F1200	44		
Moderate	Talc	70	$BaSO_4$	260	$BaSO_4$	450	Bentonite	170	$BaSO_4$	5400
	$BaSO_4$	80	Talc	920	Talc	2370	$BaSO_4$	230	Casting powder	11 700
	Bentonite	140	Bentonite	940	Bentonite	2390	Talc	390		
					Casting powder	4320	Casting powder	390		
							Coal dust	900		
High	Casting powder	310	Casting powder	1710	Coal dust	9320			Bentonite	14 900
	Coal dust	400	Coal dust	3330					Sulphur	24 800
									Coal dust	25 800
									Talc	27 900

[a]Limit of detection.

stationary, so that the same air supply and extraction system could be used. The amount of materials for a single-test run was 200 g.

This paper presents a dustiness test that uses only 6 g of material per test run and that characterized the test material by both a single-drop and a rotating drum type of challenge. The test apparatus is based on a downscaled version of the EN 15051 rotating drum while maintaining important test parameters. The test begins with a single-drop challenge and continues with a rotation of the drum performed on the same sample and collecting the generated dust on a filter. Since it was known that the instantaneous dust generation rate may vary during the rotation period and that this variation has implications for the interpretation of the test results (Hjemsted and Schneider, 1996), the instantaneous dust concentration was monitored.

MATERIALS AND METHODS

Test materials

The test materials were chosen to represent a range of particle properties. They comprised the technical nanoparticles goethite, yttria-stabilized zirconia (Y-zirconia) granules and ultrafine TiO_2 as well as pigment-grade TiO_2 to contrast the ultrafine version, corundum polishing powders Aloxite F800 and Aloxite F1200, the mineral powders bentonite and talc and fumed silica (Table 3). The bulk density determined according to EN 15051 is also shown in Table 3. Bentonite, talc and Aloxite F1200 were from the same batch as those used to provide the data for these materials quoted in EN15051.

X-ray diffraction analysis

X-ray diffraction (XRD) analysis was used for control of material composition and determination of crystallite size. The powder samples were analysed by monochromatic $Cu_{K\alpha}$ XRD analysis using a Phillips PW3710 X-ray diffractometer operated at 40-kV generator voltage and 40-nA tube current. The samples were analysed as they were, except for the granulated Y-zirconia sample, which was gently mortared in an agate mortar to prevent the particles from sliding off the sample holder during the analysis. The powder samples were placed in either alumina holders or on zero-background quartz inserts cut parallel to [0001]. The samples were run in the step mode (5 s per 0.020° 2θ) in a range between 2° and 90° 2θ depending on the analysed material. The crystallite sizes in the powder samples were determined by Rietveld analysis (Rietveld, 1967, 1969) of the powder XRD patterns using the Topas software (Bruker AXS, Madison, WI, USA). The Rietveld refinement was completed based on the crystal structures of identified phases and neglecting potential contributions from strain in the crystal lattice. The

Table 3. Specifications of the test materials

Material	XRD mineral phases, weight (%)	XRD crystallite size (nm)	Specific surface area ($m^2\ g^{-1}$)	Material density major component ($g\ cm^{-3}$)	Bulk density according to EN 15051 ($g\ cm^{-3}$)	Comments
TiO_2 ultrafine	100% rutile	18.6	100[a]	4.23–5.5[b]	0.66	
Fumed silica	>95% amorphous silica	Amorphous	15–30[a]	2.2[a]	0.26	
	Trace of quartz	<10 nm				
Bentonite	100% montmorillonite	7.8[c]	NA	2–3[b]	0.76	
Y-zirconia	72% $(Y,Zr)O_2$	26.9	15.4[a]	6.05[a]	1.5	Granules. Diameter range 10–60 μm
	28% baddeleyite	22.9				
Goethite	100% goethite	37.6	18–21[a]	4.3[b]	0.42	
Aloxite F1200	>95% corundum	91.6	NA	3.96[b]	1.1	MMAD[d] 6.0 μm, GSD 1.36
	Trace δ-θ-alumina	ND				
Aloxite F800	>95% corundum	126.9	NA	3.96[b]	1.5	MMAD[d] 13 μm, GSD 1.3
	Trace δ-θ-alumina	ND				
Talc	79% talc	149.4[c]	NA	2.58–2.83[b]	0.69	
	21% chlinochlor	119.6[c]				
TiO_2 pigment grade	98% anatase	149.7	10[a]	3.82–3.97[b]	0.70	
	2% rutile	135.5				

NA, not available; GSD, geometric standard deviation; ND, not determined; MMAD, mass median aerodynamic diameter.
[a]Data from manufacturer.
[b]Deer *et al.* (1966).
[c]Height of tabular-shaped crystallites size determined along the crystallographic (001).
[d]MMAD from Mark *et al.* (1985).

concentrations of different phases in some of the polyphase samples were also performed under the Rietveld analysis using the Topas software.

Drum design and aerosol measurement

The drum was designed to be a downscaled version of the EN 15051 rotating drum while maintaining important test parameters. The drum consists of a cylindrical part [internal diameter (i.d.) 16.3 cm, length 23.0 cm, volume 4.80 l] with a truncated cone at each end (half angle 45°, length 6.3 cm, volume 1.13 l). The total volume of the drum is 5.93 l. The drum was made of stainless steel and all inside surfaces were polished to 450 ± 50 gloss units to minimize surface adhesion and to facilitate cleaning. The drum was electrically grounded as prescribed by EN 15051. The drum contains three lifter vanes (2 × 22.5 cm). In EN 15051, a 1-min rotation at 4 rpm and eight lifter vanes are prescribed. Therefore, the present drum was operated at 11 rpm to obtain the same number of powder parcels falling per minute as in the EN 15051 test.

The total flow rate of 11 lpm through the drum was chosen in order to obtain the same average horizontal flow velocity in the cylindrical part of the drum as in the EN 15051 drum. Conditioned [50% relative humidity (RH) following EN 15051] HEPA-filtered air was supplied in excess at atmospheric pressure at the drum inlet. At the other end of the drum, air was exhausted at 9 lpm through a 20-mm i.d. tube (mean velocity in the tube = 58.4 cm s^{-1}) narrowing down to 13 mm and passed through a 90-mm diameter, 0.8-μm pore size membrane filter (Millipore AA) for particle collection (Fig. 1). The mass of collected dust was determined in a conditioned weighing room (20°C; 50% RH) using a microbalance. The detection limit (calculated as three times the standard deviation of blank filters) was 0.67 mg.

In the 20-mm i.d. exhaust tube, two 3-mm i.d. sharp-edged probes were positioned for sampling dust at 1 lpm to a TSI Model 3091 Fast Mobility Particle Sizer (FMPS) and a TSI 3321 Aerodynamic Particle Sizer (APS), respectively. Dilution and adjustment of airflow to meet the instrument sampling flow rates was achieved in the following way (see also Fig. 1). The air sample for the APS was directed vertically downwards via two 45° bends and, subsequently, diluted in two stages. In the first stage, HEPA-filtered air was added at 4 lpm as a sheath air around the sampled air and led to the second stage. The second stage was a Palas VKL-10 aerosol diluter. This diluter insured that the air was mixed before being led to the APS intake. The total dilution was 1:50. The 4-lpm dilution air in the first stage was taken from the 5-lpm exhaust of the APS from which the excess 1 lpm was vented to the atmosphere. The other probe directed the sample air vertically upwards. The sample air was mixed with 9-lpm HEPA-filtered air using a simple "T" and led to the FMPS through a conducting, flexible tube. The total dilution was 1:10. The 9-lpm dilution air was taken from the 10-lpm exhaust air of the FMPS, from which the excess 1 lpm was vented to the atmosphere (not shown in Fig. 1). The sharp-edged probes were sampling anisokinetically at a ratio (free-stream velocity)/(inlet velocity) equal to 0.25 and followed by two 45° bends. Both probes were positioned slightly off-centre, and the APS probe was placed upstream relative to the FMPS probe.

The APS measures particle size according to their aerodynamic diameter in 51 diameter classes having midpoints ranging from 0.52 to 19.8 μm. A separate class of particles smaller than 0.52 μm is also recorded but this size class was not used. The FMPS measures particles' size according to mobility diameter in 32 diameter classes having midpoints ranging from 6.04 to 523 nm. It was noted that after the default warm-up time had passed, the background concentration reading kept decreasing and that an additional 20 min was needed to insure that the concentration reading had stabilized. Both the APS and FMPS instruments were set to collect data at 1-s time resolution.

Coincidence losses in the APS were less than ∼20% at the highest concentrations encountered and the counts were not corrected. Stokes correction was not used and thus for particles >1 μm the APS

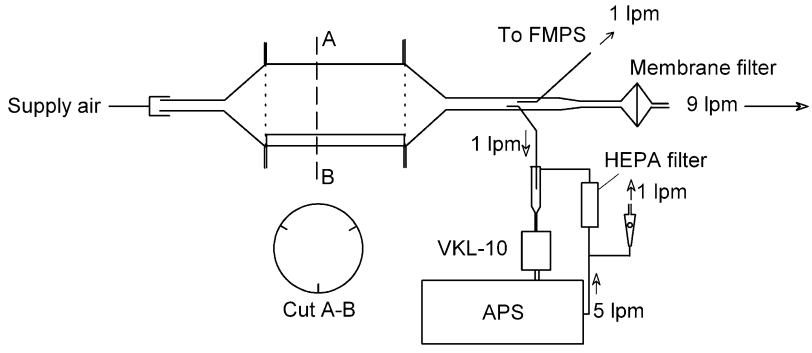

Fig. 1. Rotating drum with aerosol sampling and measurement instruments.

results overestimate the aerodynamic diameter and the overestimation increases linearly with size for diameters >1 μm. For a spherical particle with a density of ~4 g cm^{-3} (e.g. goethite, corundum) determined to have a diameter of 10 μm by the APS, the true aerodynamic diameter would be ~8 μm (Chen *et al.*, 1990).

Sampling and transport losses

While a 1-μm cut-point cyclone at the inlet of the FMPS is used to eliminate large particles, no preseparator is used in the APS. Very large particles can potentially be generated inside the drum and enter the APS. Since the study of size distribution and time-dependent dust generation rate had focus on small particles, it was decided to sample only the thoracic fraction of the dust. Sampling and transport losses were used actively to obtain this characteristic. For a given sampling and transport line configuration, the losses were estimated using the Aerosol Calculator (Baron, 2001) and making several simplifying assumptions regarding the airflow. It was, e.g. assumed that the velocity in the exit flow tube at the point of sampling was equal to the average air velocity (58.4 cm s^{-1}) in the tube. Diffusion losses could be neglected for particles >10 nm. A short section of the exit flow tube was welded to the drum and gravitational settling losses in this section were disregarded because they are reduced due to the rotation. By an iterative process, the sampling and transport line combination described above was obtained that, at least theoretically, mimicked the thoracic fraction. Koch *et al.* (1988) studied the dilution ratio of the Palas VKL-10 dilutor for particles up to 6 μm using an APS. Their results show that the dilution is very close to 10 for all particles up to ~5 μm and thus that losses can be disregarded below 5 μm. For larger particles, a potential loss in the diluter was disregarded in the calculation of transport loss.

Penetration through the stationary part of the exit tube leading to the filter was calculated also using the Aerosol Calculator assuming that the airflow had no rotating component and was laminar. The results are shown in Fig. 2. For comparison, the inhalable and thoracic conventions are shown as well as the inhalability of large particles for nose breathing in calm air at moderate exercise given by Dai *et al.* (2006). Thus, the dustiness as determined with the present method will correspond to a dustiness between the thoracic and inhalable dustiness as defined in EN 15051.

Study design and test procedure

The drum is approximately half the size of the drum used by Breum (1999) who obtained reproducible results with 25 g of test material per single run. In the present drum, the internal surface area is only one-quarter and it thus was assumed that about one-quarter of test material, i.e. 6 g, would be needed to obtain reliable results. In order to test this assumption and to test whether even smaller amounts of powder material could be used, the first part of the study was designed as a randomized trial using 2- and 6-g test material of fumed silica, TiO_2 pigment grade, TiO_2 ultrafine and Y-zirconia. The second part of the study extended the measurements using 6-g material of bentonite, talc, Aloxite F1200, Aloxite F800 and goethite. These materials were tested in random order.

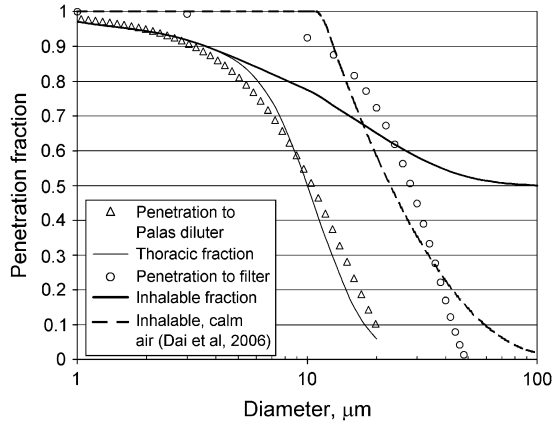

Fig. 2. Calculated penetration fractions in the aerosol sampling line to the APS (excluding the Palas diluter) and to the membrane filter. The inhalable and thoracic convention and the inhalable fraction for nose breathing at moderate exercise in calm air as given by Dai *et al.* (2006) are shown for comparison.

The test procedure was as follows. The exit cone part of the drum was removed and the drum was positioned with one of the three lifter vanes in the lowest position. Then, a weighed amount of test material was placed in a pile at the centre and at the upward moving side of the lowest lifter vane. The drum was assembled, and the three sampling pumps (FMPS, APS, filter) were turned on. After 120 s, the particle concentration was down to background levels and 180 s after starting the sampling pumps, the single-drop part of the dustiness test was performed by rotating the drum exactly 180° at 11 rpm and then stopping. After a 180-s pause, the drum was rotated at 11 rpm for 60 s and then stopped. After the drum was stopped, sampling continued for another 120 s and then the sampling pumps were turned off. This completed the rotation part of the dustiness test. Then, the drum was disassembled. The remaining material was poured out and the remaining loose material was removed by tapping on the drum as specified in EN 15051. The tips of the sampling probes for the FMPS and APS were cleaned with compressed CO_2, and the FMPS cyclone chamber was wiped with ethanol-wetted, lint-free paper. The entire cycle was repeated four times, where the first run served to saturate the internal surface of the drum (Burdett *et al.*, 2000). Between change of amount or type of material, an

additional cleaning procedure was implemented comprising wet wiping of the drum and replacing the grease on the bottom plate of the cyclone coarse fraction chamber with clean grease.

The EN 15051 prescribes that the material be tested as received. This procedure was followed despite that moisture content affects dustiness as determined by a continuous drop method (Plinke *et al.*, 1995). However, some equilibration will take place during the 180-s exposure to the 50% RH air after the drum has been assembled and before the single drop is actuated.

Data analysis

A typical time trace is shown in Fig. 3. About 6 s after starting the drum, an instantaneous and steep rise in concentration was observed. For the single drop, this time is termed t_{single} and for the rotation test t_{rotation}, both given in units of seconds. For determination of size distributions and dustiness, the particle number concentration readings, N_i, for every second were integrated

$$\text{IN}_{\text{single}} = \sum_{t_{\text{single}}}^{t_{\text{single}}+120} N_i(\text{cm}^{-3}),$$
$$\text{IN}_{\text{rotation}} = \sum_{t_{\text{rotation}}}^{t_{\text{rotation}}+180} N_i(\text{cm}^{-3}). \quad (1)$$

for both the FMPS and the APS data. Calculations were made for each diameter interval, but the diameter has been left out from the equations for sake of clarity. All FMPS and APS measurements were corrected for background by using the average counts during the time period $t_{\text{single}} - 46$ to $t_{\text{single}} - 6$ s. A log-normal mobility diameter distribution was fitted to $\text{IN}_{\text{single}}$ and $\text{IN}_{\text{rotation}}$ for the FMPS data. This mode is fully characterized by the total integrated number (IN) concentration, in the mode, the number geometric mean diameter (GMD) and the geometric standard deviation. For the APS data, similar calculations were made, but a bimodal log-normal aerodynamic diameter distribution was fitted. It was not meaningful to fit still larger diameter modes to the APS data because of the upper size cut-off (Fig. 2).

From the data, it was found that at time $t = t_{\text{rotation}}+180$ s, the concentration was always $<2\%$ of the peak. Total number of generated particles, S, was thus calculated as:

$$S_{\text{single}} = \text{IN}_{\text{single}} \times Q, \quad S_{\text{rotation}} = \text{IN}_{\text{rotation}} \times Q, \quad (2)$$

where Q is the total flow rate per second (11 lpm) and since the data were sampled once per second. S was calculated for the single-drop and the rotation test, respectively, and both for the FMPS and the APS data.

The respirable volume of particles was calculated in the following way. For each diameter interval, IN was multiplied by the corresponding volume using mobility diameter for the FMPS data and aerodynamic diameter for the APS data and by the respirable convention and finally adding the results across all diameter intervals.

The dustiness index determined by the filter method was calculated as the total mass collected on the filter in milligrams divided by the mass of the test sample in kilograms. The mass determined on the filter sample was multiplied by a factor of 11/9 to adjust for the difference in the total airflow (11 lpm) in the drum to airflow through the filter (9 lpm). It was disregarded that the sampling probes for the FMPS and APS were not sampling isokinetically thereby under-sampling large particles leading to an overestimation of the dustiness index based on the filter measurements. The sampling probes have a minimum sampling efficiency of $(3\text{ mm})^2/(20\text{ mm})^2$ for very large particles. Thus, the largest possible overestimation would be by the factor $\left(1 - \left(\frac{3}{20}\right)^2 - \left(\frac{3}{20}\right)^2\right) \times \frac{11}{9} = 1.17$. As previously mentioned, the first of the four runs served to condition the interior surface of the drum and the results from the first run were not included. Indeed, the various concentration measures showed a tendency to be lower for the first run than the average of the following three runs.

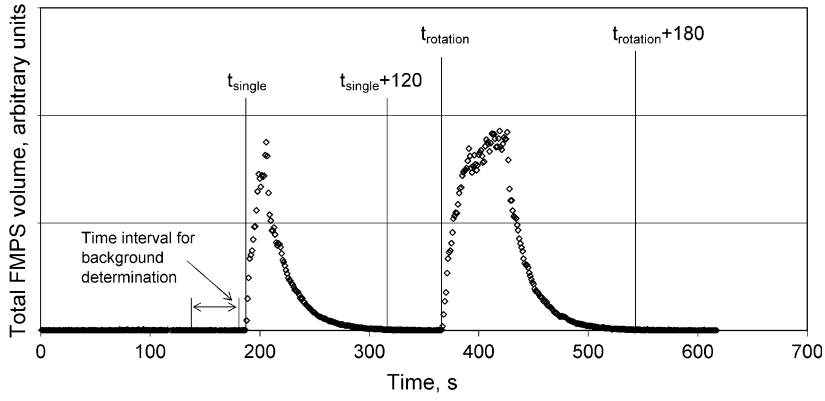

Fig. 3. Time profile of total particle volume as measured by the FMPS for ultrafine TiO_2, 6-g material.

Inverse digital filtering (Hjemsted and Schneider, 1996) was used to calculate the dust generation rate at time i, R_i, in units of total amount per time. The equation was

$$R_i = k(C_i - C_{i-1}e^{-\frac{1}{\tau}}), \quad (3)$$

where k is drum volume, C is concentration and τ is the time constant. At a volume flow rate of 11 lpm, the nominal time constant for the air exchange in the drum is 32 s.

RESULTS

The results obtained from the testing of 2-g sample material (data not shown) had coefficients of variation (CV) that were both smaller and larger than the corresponding CV's for the 6-g sample tests. For the four materials (fumed silica, TiO_2 pigment grade and ultrafine, and Y-zirconia) in the rotation test, there was a decreasing trend in the dustiness per mass unit for increasing sample mass for the number of particles in the FMPS size mode, the combined APS size modes and the respirable volume when normalized by mass of test material as well as for the dustiness index as determined by the filter method. Only four of the total of 16 comparisons between 2- and 6-g tests gave differences that were statistically significant (two-sample t-test at $P = 0.1$. Using the conservative Bonferroni correction 1/16, this corresponds to $P = 0.006$ for each individual comparison). For the four significant differences, the 6-g samples resulted in a dustiness (per mass unit) ranging from ~70 to ~90% of the dustiness for 2-g samples. Only the results obtained from the test of 6-g sample material are further reported.

Due to the inconsistent results and the large scatter in counts above background for particles below ~50 nm, it is uncertain whether particles below 50 nm were generated by any of the powders. Figure 4 shows the size distributions of the generated particles for selected materials obtained from the rotation test. All size distributions as measured by the APS were bi- or multimodal. The GMD of the size modes are given in Table 4. In the FMPS size range, no particles could be detected above background for TiO_2 pigment grade and due to low counts no distinct size mode could be identified for Aloxite F1200. Table 4 shows that the GMDs for the single-drop and the rotation test were identical, except that Aloxite F800 had smaller GMD for the single-drop than for the rotation test.

Figure 5 shows the ratio of respirable mass generated during the single-drop testing to the generation during single-drop and rotation testing combined. This ratio was taken to be equal to the ratio of the

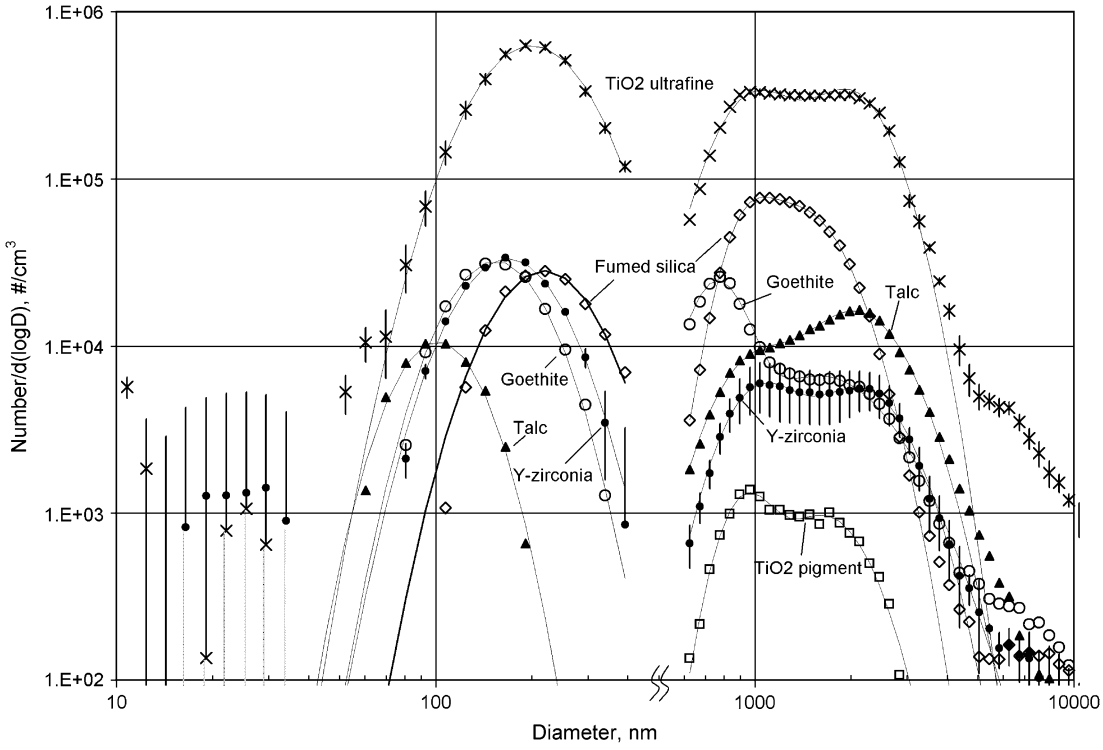

Fig. 4. Size distributions for selected materials obtained from the rotation test (IN per cubic centimetre). Means and for ultrafine TiO_2 and Y-zirconia also standard deviation ($n = 3$). Curves are the mean of the fitted distributions ($n = 3$). The two largest FMPS and the two lowest APS diameter channels are not shown due to uncertainty in the counting efficiency.

Table 4. GMD of the fitted log-normal size modes based on the INs

	Fumed silica		TiO_2 pigment		TiO_2 ultrafine		Y-zirconia		Bentonite		Talc		Aloxite F1200		Aloxite F800		Goethite	
	Mean	CV (%)	Mean	CV (%)	Mean	CV (%)	Mean	CV (%)	Mean	CV (%)	Mean	CV (%)	Mean	CV (%)	Mean	CV (%)	Mean	CV (%)
FMPS single drop	220	2	nd	nd	196	1	168	5	214	2	102	3	nd	nd	202	2	159	4
FMPS rotation	219	0	nd	nd	200	1	168	0	213	1	101	2	nd	nd	205	1	154	1
APS small mode, single drop	959	2	893	3	1004	1	1201	21	1101	2	1024	2	1811	4	1280	5	758	2
APS small mode, rotation	960	2	937	2	1014	1	1059	5	1059	0	1008	1	1818	1	1664	1	757	1
APS large mode, single drop	1358	2	1589	3	1958	0	2267	9	1924	2	2108	0	2503	1	2455	2	1613	30
APS large mode, rotation	1360	2	1646	3	1981	1	2151	7	1862	0	2073	1	2493	0	2564	1	1603	4

nd, no mode could be identified; mean and CV ($n = 3$).

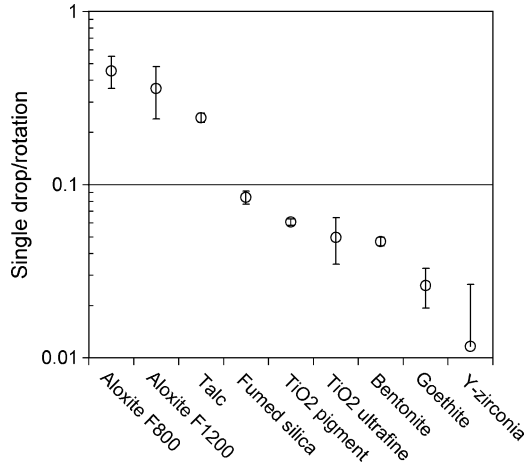

Fig. 5. Mass ratios between respirable dust emitted during single-drop test and during single-drop and rotation test combined. Mean and standard error of mean ($n = 3$).

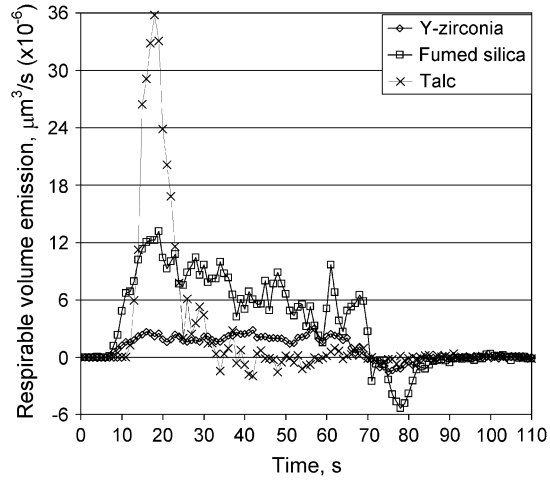

Fig. 6. Representative time profiles of dust generation rate, R, for Y-zirconia, fumed silica and talc during rotation test. Data were smoothed by a moving 10-s average (5 s for talc; thus, the apparent time difference in concentration rise).

respirable volumes as determined from the FMPS and APS data since the single-drop and the rotation test gave almost identical size distributions and thus the density and shape factor does not enter the equation.

Three different types of dust generation rate time profiles, R_i, were observed and are shown in Fig. 6. Talc emitted most of the dust during a short initial burst. Notice that the peak appears broader than it would be in reality because Fig. 6 shows the 5-s moving average in order to reduce the random fluctuations. A similar burst was found for Aloxite F1200 and Aloxite F800. These three materials had the highest ratios shown in Fig. 5. For fumed silica, TiO_2 ultrafine and pigment grade, and bentonite the generation rate declined during the 1-min rotation period while it was virtually constant for Y-zirconia and for goethite. The latter two materials had the lowest ratios shown in Fig. 6. The dust generation rate shown in Fig. 6 was initially calculated using the nominal time constant τ in equation (3). However, this produced negative values for talc, Aloxite F1200 and Aloxite F800 during rotation. Thus, the time constant was reduced until no negative values were obtained. This occurred at $\tau = 20$ s for all three materials and this value was used for the calculations.

The number of particles generated during the single-drop, S_{single}, and the rotation test, $S_{rotation}$, is shown in Table 5 and the dustiness index determined by the mass collected on the filter is shown in Table 6.

DISCUSSION

The tests performed with the 2-g samples gave reproducible results. By using a standard weight of 6-g sample material, even powder materials with much lower dustiness than the present can be tested. Dustiness showed a decreasing trend with increasing mass of test material. However, the influence of mass of test material on the dustiness index determined with a rotating drum appears to be complex, and both

Table 5. Total number, S, of particles ($\times 10^{-7}$) emitted in the FMPS size mode and the two APS size modes combined

	Fumed silica		TiO_2 pigment		TiO_2 ultrafine		Y-zirconia		Bentonite		Talc		Aloxite F1200		Aloxite F800		Goethite	
	Mean	CV (%)	Mean	CV (%)	Mean	CV (%)	Mean	CV (%)	Mean	CV (%)	Mean	CV (%)	Mean	CV (%)	Mean	CV (%)	Mean	CV (%)
S_{single} FMPS	1.3	18	nd	nd	20.6	36	0.63	109	2.5	18	1.7	14	nd	nd	0.69	26	0.38	36
$S_{rotation}$ FMPS	14.3	5	nd	nd	344.8	6	17.1	2	45.5	1	4.6	19	nd	nd	0.82	33	15.5	3
S_{single} APS	2.6	13	0.05	3	17.2	39	0.06	10	4.2	5	3.5	2	1.3	19	1.4	46	0.25	9
$S_{rotation}$ APS	39.4	12	0.75	10	264.3	4	4.8	29	85.6	4	11.2	13	2.9	69	2.1	38	11.2	8

nd, no mode could be identified. Mean and CV ($n = 3$).

positive and negative associations with mass have been reported (Breum, 1999; Burdett *et al.*, 2000). EN 15051 prescribes use of a standard volume of material and it has been argued (Burdett *et al.*, 2000) that use of a standard volume would make the dynamics of dust production more consistent. For the materials having the highest and lowest bulk density (Table 3) and the highest and lowest dustiness (Tables 5 and 6), the dustiness test was made for both 2- and 6-g samples. Since the results showed only a minor effect of sample mass on dustiness (per unit mass), it is likely that use of a standard volume would have resulted in findings similar to the present.

The log-normal distribution fitted the FMPS data well (Fig. 4). Also the bimodal log-normal size distribution fitted the APS data below ~4 μm. The GMDs of the size modes were very reproducible (Table 4). Thus, each of the size modes can be reliably identified and quantified and the results used for dustiness characterization. The FMPS and the APS have different measurement principles and the diameter ranges do not overlap. It thus is no simple matter to directly compare the modes, i.e. to merge the size distributions obtained by the FMPS and the APS into one. Since such a comparison is not of primary importance for characterization of dustiness, it was not attempted to merge the distributions.

The submicron size modes were very distinct and this was somewhat surprising. The separation from the larger size modes occurred at a diameter that coincided with the diameter that separates the measuring ranges of the two instruments. Thus, part of this distinct separation of modes could be due to reduced counting efficiency of both instruments close to 500 nm. For the APS 3321, Volckens and Peters (2005) reported an efficiency of 85–99% in the diameter range 0.8–9.4 μm for solid particles, but gave no data for smaller diameters. No absolute measurements of the counting efficiency of the FMPS have been published. However, very recently results of challenging four mobility analyzers including the FMPS with aerosols of NaCl and diesel soot have been presented (Asbach *et al.*, 2007). They found that the instrument responses differed to a degree dependent on particle size and depending on type of aerosol. It thus cannot be excluded that the FMPS used in the present study may have underestimated the concentration in the uppermost diameter intervals. In consequence, Fig. 4 shows the results excluding the two highest diameter channel for the Scanning Mobility Particle Sizer (SMPS) and the two lowest for the APS.

Pagels *et al.* (2005) reported that the APS 3321 generated phantom peaks at ~3 and 8 μm in the volume-weighted distribution if there were extremely high particle concentrations of particles with GMD of ~0.3 μm. Converting the ratio of the peak heights as read from their graphs to a corresponding ratio for the number distribution resulted in a value of three orders of magnitude. Occurrence of such phantom peaks could thus be disregarded for the present conditions.

Similar size modes have also been found by others. Maynard (2002) tested ultrafine TiO_2 powder (specific surface area 50 ± 15 m^2 g^{-1}) by the fluidization method. Using a TSI SMPS and a TSI APS 3320 in parallel, a bimodal size distribution was found with the fitted bimodal log-normal size distribution having modes 333 and 1800 nm. Size analysis by transmission electron microscopy confirmed the distribution was bimodal. A bimodal distribution was also found for nanostructured aluminium oxide powder using the same test (Baron *et al.*, 2003). Bohgard *et al.* (1994) measured the size distribution of particles when handling an amorphous SiO_2 powder (Aerosil™), nominal particles size 7 nm. The size distribution in the range 20–1000 nm measured with a differential mobility analyzer (TSI) had a number mode ~120 nm. The distribution had a minimum at ~500 nm. The size distribution in the range 1–10 μm had a number mode at ~1.3 μm as measured with an APS (TSI). Interestingly, for an aerosol generated from single-walled carbon nanotubes using the two-component vortex shaker fluidized bed method, three size modes were found for a test of 5-min duration: one mode close to 1800 nm for APS counts and one mode in the range 100–300 nm and one mode below 30 nm for the SMPS counts (Baron *et al.*, 2003).

The current test generated two more or less separated size modes >0.9 μm and in addition all materials except TiO_2 pigment grade and Aloxite F1200 generated a size mode in the range from ~100 to ~220 nm. When comparing the material mean

Table 6. Dustiness (±standard error, $n = 3$) in milligrams per kilogram of test material determined by the present filter method[a] and as quoted for the same materials in CEN (2006)

	TiO_2 pigment	Aloxite F800	Y-zirconia	Aloxite F1200		Fumed silica	Goethite	Talc		Bentonite		TiO_2 ultrafine
				Thoracic	Inhalable			Thoracic	Inhalable	Thoracic	Inhalable	
Present	31 ± 21	278 ± 79	283 ± 43	448 ± 171		702 ± 291	942 ± 218	1347 ± 85		1710 ± 206		8338 ± 233
CEN (2006)	—	—	—	140	170	—	—	920	2370	940	2390	—

[a]This dustiness is between the thoracic and inhalable dustiness as defined in EN 15051 (Fig. 2).

Fig. 7. Total number of particles generated, *S*, during rotation test (in FMPS size mode and in the two APS size modes combined) and dustiness index (mg kg^{-1}). When a material consisted of two mineral phases, the mean crystallite size was calculated as the mass-weighted average of the crystallite size for each phase. Y-error bars are standard error of mean.

crystallite size (leaving out the amorphous fumed silica and Aloxite F1200 because no mode could be identified) with the GMD in this rather narrow range, no obvious relationship could be found. However, from Fig. 7, it is seen that for increasing crystallite size there is a decreasing trend for the total number of emitted particles during the rotation test and for the dustiness index.

The results of the present and other studies (Bohgard *et al.*, 1994; Maynard, 2002; Baron *et al.*, 2003; Kuhlbusch *et al.*, 2004) suggest that airborne particles generated during handling of ultrafine powders and powders of engineered nanoparticles are agglomerates/aggregates. Nanoparticles have a natural tendency to aggregate due to the significant attractive forces between nanosized particles and processing of nanosized powders by fluidization can be used to form large, spherical aggregates in order to modify their properties (Hakim *et al.*, 2005). Agglomeration and aggregation is also influenced by humidity, temperature, pressure and storage time (Brockel *et al.*, 2006). Insoluble particles may aggregate or agglomerate owing to cohesion, adsorption of moisture and liquid bridge formation (Brockel *et al.*, 2006), and clays, such as bentonite, may show particle growth or aggregation owing to humidity-induced dissolution–precipitation processes (e.g. Szepvolgyi *et al.*, 2001; Gbureck *et al.*, 2005; Brockel *et al.*, 2006). These factors (as influenced by preceding handling, transport and storage conditions) were only partially controlled in the present study, and thus may have affected both the amount and size distribution of the particles generated during the test. Studies of coarse particles, relevant for the pharmaceutical industry, have shown that dustiness of these particles is highly related to the morphology of the primary particles (Pujara, 1997). It is unknown whether this

relationship can be extrapolated from the micrometer region into the nanosize region.

Dustiness as quantified by particle number (Table 5) and by the mass-based dustiness index (Table 6) had a large range. The lowest dustiness was found for TiO_2 pigment and the largest for TiO_2 ultrafine and the difference was about a factor 350 for the total particle number in the two APS size modes and about a factor 280 for the mass-based dustiness index. In the FMPS size range, ultrafine TiO_2 had the highest dustiness while none could be detected for the pigment grade. These findings suggest a corresponding large difference in exposure potential. In particular, they suggest that preventive measures would have to be much stricter if the pigment-grade TiO_2 were to be replaced by the ultrafine version. Maynard (2002) showed that aggregates of ultrafine TiO_2 were broken up during shaking in a synthetic lung fluid, even though not into primary particles. Thus, in addition to the increased dustiness in number of particles, there could be an additional potential risk caused by the de-agglomeration of the ultrafine TiO_2 particles in the lung fluids.

The existence of different dust generation rate time profiles as shown in Fig. 6 has also been found by others (Hjemsted and Schneider, 1996). The initial burst shown for talc in Fig. 6 might have been even more pronounced, had the test not been preceded by the single-drop test. This difference in the dynamics of dust generation is reflected in differences in the ratios between the respirable mass generated during the single-drop and during the rotation test and thus is one factor influencing the difference in ranking of dustiness as determined by a single-drop and a rotating drum method.

Visual observation showed that during the 180° rotation of the drum during the single-drop test, dust may slide off the lifter vane in a continuous flow (of short duration) rather than an instantaneous drop at a given angle of rotation. Thus, the present single-drop test is a hybrid of the single-drop and the continuous single-drop method with the important modification that the dust does not impact on a dust pile that gradually would build up in the continuous single-drop test and that the drop height is dependent on the adhesion and flowability of the material.

The nominal time constant of 32 s for the air exchange in the drum did not fit the data and had to be lowered to an apparent time constant of 20 s. A similar finding was made by Hjemsted and Schneider (1996). Since the fitted value was determined for the materials emitting particles in an initial short burst, this could indicate that the amount of material falling was reduced for these powders due to wall adhesion. A more likely cause could be that there is incomplete mixing in the drum. Thus, it would not be possible to reliably extract the dust generation rate caused by the first drop of the material solely from an analysis of the time profile for the initial phase of a rotation test. The present approach can extract information on dust generation during the first fall of the material in addition to the continuous rotation condition in one test and is thus an easy method for obtaining a more detailed characterization of dustiness in relation to various handling scenarios.

The dustiness as determined with the present filter method is between the thoracic and inhalable dustiness (Fig. 2). Table 6 could suggest that the present rotating drum test generates results that are within the same order of magnitude as the benchmark values given in EN 15051 for the rotation test. The ratio between the single-drop test to the single-drop and rotating test combined for respirable dustiness ranged a factor of ~40 (Fig. 5). A similar range when comparing the two methods given in EN 15051 thus could be expected.

As discussed by Liden and Harper (2006), an additional definition of inhalablility for calm air conditions may be needed, and the outlet of the present drum could likely be modified so that the filter would collect particles according to such a future new inhalability criterion.

In conclusion,

1. The single-drop and the rotating drum part of the dustiness test using 6 g of test material gave very reproducible results both in terms of amount and size distribution of the generated particles.
2. The generated particles had two more or less separate size modes >0.9 μm and except for TiO_2 pigment grade and Aloxite F1200 also a size mode in the range from ~100 to ~220 nm.
3. For increasing crystallite size, a decreasing trend was found for total number of generated particles during the rotation test and for dustiness index.
4. TiO_2 pigment grade had the lowest dustiness and TiO_2 ultrafine the highest dustiness and being about a factor 300 times larger.
5. The dynamics of the dust generation could be visualized by extracting the dust generation rate from the concentration time profiles and showed three types of profiles: a brief initial burst, a declining rate and a constant rate.
6. The new test provides an easy method for a more detailed characterization of dustiness in relation to various handling scenarios than a single-drop or a rotation test alone.

FUNDING

The Nordic Council of Ministers (411050-60091).

Acknowledgements—We wish to thank Associate Professor T. Balic-Zunic and technician H. Almind at the University of Copenhagen, Denmark, for conducting the XRD analysis and Rietveld refinement.

REFERENCES

Asbach C, Kaminski H, Fissan H *et al*. (2007) Intercomparability of continuous particle number based measurement techniques for nanotechnology workplaces. Poster presented at EuroNanoForum 2007. Nanotechnology in Industrial Applications. June 19–21, 2007, CCD Düsseldorf, Germany.

Baron P. (2001) Aerosol calculator, version 01-okt-01. Available at:http://www.bgiusa.com/cau/aerocal8.zip. Accessed 21 August 2006.

Baron PA, Maynard AD, Foley M. (2003) Evaluation of aerosol release during the handling of unrefined single walled carbon nanotube material. NIOSH. DART-02-191 Rev.1.1 April 2003. Cincinnati, OH: NIOSH. Available at:http://frictioncenter.engr.siu.edu/Media/NIOSH%20%20DART-02-191%20r1-1%20med%20res.pdf. Accessed 21 August 2006.

Bohgard M, Anderber MT, Ekholm A-K. (1994) Source characteristics of emitted aerosol in the size range 0.02 to 10μm at pigment handling in dye manufacturing. J Aerosol Sci; 25(Suppl. 1): S461–2.

Boundy M, Leith D, Polton T. (2006) Method to evaluate the dustiness of pharmaceutical powders. Ann Occup Hyg; 50: 453–8.

Breum NO. (1999) The rotating drum dustiness tester: variability in dustiness in relation to sample mass, testing time, and surface adhesion. Ann Occup Hyg; 43: 557–66.

Breum NO, Schneider T, Jørgensen O *et al*. (2003) Cellulosic building insulation vs mineral wool, fiberglass or Perlite: installer's exposure by inhalation of fibers, dust, endotoxin and fire retardant additives. Ann Occup Hyg; 47: 653–69.

Brockel U, Wahl M, Kirsch R *et al*. (2006) Formation and growth of crystal bridges in bulk solids. Chem Eng Technol; 29: 691–5.

Brouwer DH, Links IH, De Vreede SA *et al*. (2006) Size selective dustiness and exposure; simulated workplace comparisons. Ann Occup Hyg; 50: 445–52.

Burdett GJ, Chung KYK, Mark D *et al*. (2000) Development of a method for dustiness testing. EU contract SMT4-CT96-2074. HSE report IR/L/MF/00/11. Sheffield, UK: Health and Safety Laboratory.

Cashdollar KL. (2000) Overview of dust explosibility characteristics. J Loss Prev Process Ind; 13: 183–99.

CEN. (2006) EN 15051 Workplace atmospheres—measurement of the dustiness of bulk materials—requirements and reference test methods. Brussels, Belgium: European Committee for Standardization.

Chen BT, Cheng YS, Yeh HC. (1990) A study of density effect and droplet deformation in the TSI Aerodynamic Particle Sizer. Aerosol Sci Technol; 12: 278–85.

Dai Y-Y, Juang Y-J, Wu Y-Y *et al*. (2006) *In vivo* measurement of inhalability of ultralarge aerosol particles in calm air by humans. J Aerosol Sci; 37: 967–73.

Deer WA, Howie RA, Zussman JU. (1966) An introduction to rock-forming minerals. New York: Longman Scientific & Technical.

DIN. (2006) DIN 55992-1. Determination of a parameter for the dust formation of pigments and extenders—Part 1: rotation method [in German]. Berlin, Germany: DIN Deutsches Institut für Normung, Beuth Verlag.

Eckhoff RK. (2005) Current status and expected future trends in dust explosion research. J Loss Prev Process Ind; 18: 225–37.

Gbureck U, Dembski S, Thull R *et al*. (2005) Factors influencing calcium phosphate cement shelf-life. Biomaterials; 26: 3691–7.

Gill TE, Zobeck TM, Stout JE. (2006) Technologies for laboratory generation of dust from geological materials. J Hazard Mater; 132: 1–13.

Hakim LF, Portman JL, Casper MD *et al*. (2005) Aggregation behaviour of nanoparticles in fluidized beds. Powder Technol; 160: 149–60.

Hamelmann F, Schmidt E. (2004) Methods for characterizing the dustiness estimation of powders. Chem Eng Technol; 27: 844–7.

Hjemsted K, Schneider T. (1996) Documentation of a dustiness drum test. Ann Occup Hyg; 40: 627–43.

HSE. (1996) MDHS 81 Dustiness of powders and materials. Methods for the determination of hazardous substances. Sudbury, UK: Health and Safety Laboratory, HSE Books.

Koch W, Lödding H, Mölter W *et al*. (1988) Dilution system for aerosol measurements with optical particle counters at very high concentrations [in German]. Staub Reinhalt Luft; 48: 341–4.

Kuhlbusch TAJ, Neumann S, Fissan H. (2004) Number size distribution, mass concentration, and particle composition of PM1, PM2.5, and PM10 in bag filling areas of carbon black production. J Occup Environ Hyg; 1: 660–71.

Liden G. (2006) Dustiness testing of materials handled at workplaces. Ann Occup Hyg; 50: 437–9.

Liden G, Harper M. (2006) Analytical performance criteria. The need for an international convention for inhalable dust in calm air. J Occup Environ Hyg; 3: D94–101.

Madsen AM, Kruse P, Schneider T. (2006) Characterization of microbial particle release from biomass and building material surfaces for inhalation exposure risk assessment. Ann Occup Hyg; 50: 175–87.

Mareels J, Pensis I. (2006) IMA Dustiness Project. CEN/TC137/WG3/N398. Brussels, Belgium: European Committee for Standardization.

Mark D, Vincent JH, Gibson H *et al*. (1985) Applications of closely graded powders of fused alumina as test dusts for aerosol studies. J Aerosol Sci; 16: 125–31.

Maynard AD. (2002) Experimental determination of ultrafine TiO2 deagglomeration in a surrogate pulmonary surfactant: preliminary results. Ann Occup Hyg; 46(Suppl. 1): 197–202.

Maynard AD, Baron PA, Foley M *et al*. (2004) Exposure to carbon nanotube material: aerosol release during the handling of unrefined single-walled carbon nanotube material. J Toxicol Environ Health A; 67: 87–107.

Pagels J, Gudmundsson A, Gustavsson E *et al*. (2005) Evaluation of aerodynamic particle sizer and electrical low-pressure impactor for unimodal and bimodal mass-weighted size distributions. Aerosol Sci Technol; 39: 871–87.

Plinke MAE, Leith D, Boundy MG *et al*. (1995) Dust generation from handling powders in industry. Am Ind Hyg Assoc J; 56: 251–7.

Pujara CP. (1997) Determination of factors that affect the generation of airborne particles from bulk pharmaceutical powders. Thesis, UMI number 9808505. Ann Arbor, MI: Purdue University Graduate School, UMI.

Rietveld HM. (1967) Line profiles of neutron powder-diffraction peaks for structure refinement. Acta Crystallogr; 22: 151–2.

Rietveld HM. (1969) A profile refinement method for nuclear and magnetic structures. J Appl Crystallogr; 2: 65–71.

Szepvolgyi J, Mohai I, Gubicza J. (2001) Atmospheric ageing of nanosized silicon nitride powders. J Mater Chem; 11: 859–63.

Volckens J, Peters TM. (2005) Counting and particle transmission efficiency of the aerodynamic particle sizer. J Aerosol Sci; 36: 1400–8.